Energy-pooling collisions in barium

J. A. Neuman, A. Gallagher,* and J. Cooper
Joint Institute for Laboratory Astrophysics, University of Colorado and National Institute of Standards and Technology, Boulder, Colorado 80309-0440
(Received 7 March 1994)

Rate coefficients for energy-pooling collisions between low-lying excited states of Ba have been measured. The $6s6p(^3P_1)$ level in Ba is pumped by a cw diode laser, and radiative decay and collisions with buffer-gas atoms also populate the $5d6s(^1D)$ and $5d6s(^3D)$ metastable levels. The densities of these low-lying excited states are measured by the absorption of lines from a Ba hollow-cathode lamp, and the states populated by energy-pooling collisions are studied by comparing their fluorescence intensity to that of the laser-excited level. The rate coefficients are on the order of gas-kinetic rates, and they are not strongly dependent on energy defect, spin changes, or angular-momentum changes.

PACS number(s): 34.30.+h, 34.50.−s

I. INTRODUCTION

Energy pooling refers to the transfer of electronic energy when two excited atoms collide to produce one highly excited atom and one ground-state atom. Energy pooling (EP) provides a particularly useful tool for studying energy-transfer collisions, and it is of interest since it may lead to an increased understanding of interatomic interactions and collision dynamics. Since both collision partners are optically excited, EP offers a unique possibility to control such collision parameters as polarization and spin. It has also been proposed that EP can be used to create population inversions and to populate high-lying levels that would be difficult to excite directly. Although EP has been studied extensively in alkali-metal atoms [1–3], alkaline earth metals [4–6], group II B elements [7], and heteronuclear systems [8], EP in barium has not yet been reported.

In the present experiment, the 791-nm barium intercombination line is excited by a grating-cavity tuned cw diode laser. The laser-excited $6s6p(^3P_1)$ level (henceforth referred to as the $6P$ level) and the collisionally and radiatively produced lower-lying metastable $6s5d(^{2S+1}D_J)$ levels (abbreviated as the $5D$ levels) contribute to energy pooling, and the following processes have been observed:

$$\mathrm{Ba}^*(6\,^3P_1)+\mathrm{Ba}^*(6\,^3P_1)\rightarrow \mathrm{Ba}(6\,^1S_0)+\mathrm{Ba}^{**}(n\,^{2S+1}L)\pm\Delta E\ , \quad (1)$$

$$\mathrm{Ba}^*(5\,^1D_2)+\mathrm{Ba}^*(5\,^1D_2)\rightarrow \mathrm{Ba}(6\,^1S_0)+\mathrm{Ba}^{**}(n\,^{2S+1}L)\pm\Delta E\ , \quad (2)$$

$$\mathrm{Ba}^*(5\,^3D_J)+\mathrm{Ba}^*(5\,^3D_J)\rightarrow \mathrm{Ba}(6\,^1S_0)+\mathrm{Ba}^{**}(n\,^{2S+1}L)\pm\Delta E\ , \quad (3)$$

where Ba* represents the $6P$ and $5D$ levels, and Ba** signifies the levels produced by the energy-pooling collisions of the Ba* atoms. Although other EP collisions may occur, they have not been isolated. We will ignore the different J levels of the $5\,^3D_J$ state, with $\mathrm{Ba}^*(5\,^3D_J)$ referring to the J sum over an equilibrium J distribution. The relevant Ba energy levels and the Ba* pair energies are included on the energy-level diagram in Fig. 1.

The rate equation for EP is examined first, since the analysis of this equation establishes the measurements necessary for a determination of an EP rate coefficient. Then, a description of the experimental apparatus is presented. Since it is necessary to resolve the contribution to energy pooling from several different Ba* states, the ratios of the different Ba* densities are varied, allow-

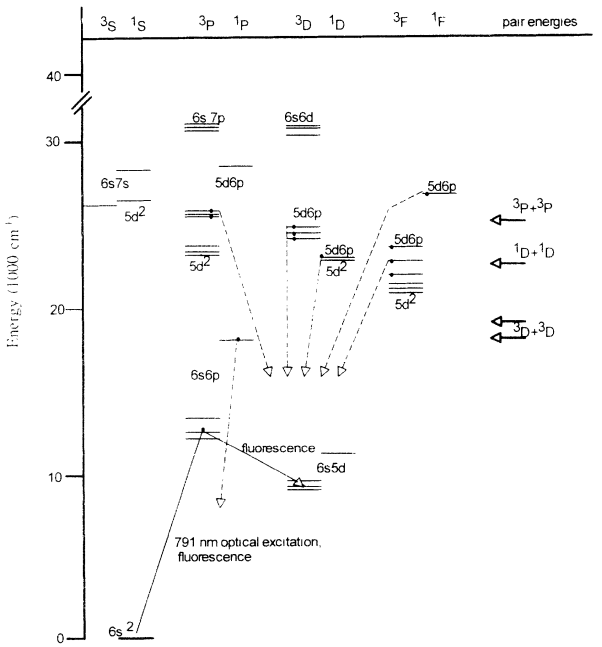

FIG. 1. Barium energy-level diagram with relevant pair energies. The dashed lines indicate observed EP fluorescence.

*Also at Quantum Physics Division, National Institute of Standards and Technology, Boulder, CO.

ing processes (1), (2), and (3) to be isolated. Thus, the production, losses, spatial distribution, and buffer gas dependence of the different Ba* levels are discussed next. Finally, the fluorescence intensity from the levels populated by EP is correlated to collisions between isolated Ba* levels, and rate coefficients are determined.

II. RATE EQUATION

A solution to the rate equations for excited-state densities determines which variables must be measured to yield a rate coefficient for EP. Since the excitation is cw, a steady-state solution to the rate equations yields the desired rate coefficients. The EP rate coefficient must be defined carefully. This work follows the convention established by Kelly, Harris, and Gallagher [4]. Ordinarily, the rate coefficient k for collisions between two atoms in states 1 and 2 (with densities n_1 and n_2) is defined by

$$R = k_{12} n_1 n_2 ,$$

where R is the collisional rate per volume. For collisions in a cell, a factor of $\frac{1}{2}$ is included to prevent double counting each colliding pair of identical atoms:

$$R = \tfrac{1}{2} k_{11} n_1^2 .$$

We will consider the simplified case of only one type of Ba* state and a Ba** state that is produced only by energy pooling and lost only by radiative decay. Assuming no other collisional or radiative populating and depopulating processes or diffusive losses to the walls, an appropriate rate equation is

$$\frac{d}{dt}\int n^{**}(V)dV = -\frac{\int n^{**}(V)dV}{\tau^{**}} + \frac{k}{2}\int n^{*2}(V)dV , \tag{4}$$

with the steady-state solution of

$$k = \frac{2}{\tau^{**}} \frac{\int n^{**}(V)dV}{\int n^{*2}(V)dV} . \tag{5}$$

Here, k is the rate coefficient for the collisional production of highly excited Ba** atoms (with density n^{**} and radiative lifetime τ^{**}) from the collision of Ba* atoms (with density n^*). Integrals of the density over the cell volume (V) are used because different Ba*and Ba** states have dramatically different spatial distributions within the cell. In particular, the metastable $5D$ states are distributed over much of the cell while the $6P$ states are confined mostly to the laser volume.

A determination of absolute rate coefficients requires the knowledge of n^*, which is obtained from absorption of light from a barium hollow-cathode lamp. Since n^{**} created by EP is too low (about 10^{-5} of n^*) to be easily determined in this fashion, n^{**} is obtained by comparing the Ba** fluorescence intensity to the fluorescence intensity from the 791-nm intercombination line $[6s^2(^1S_0) \rightarrow 6s6p(^3P_1)]$. The $6s6p(^3P_1)$ and Ba** atoms are confined to a small volume in the center of the cell, whereas the fluorescence from these atoms can be reabsorbed throughout the cell. Thus, the transmission (T) of fluorescence intensity through the barium vapor cannot be omitted. Since the detection system images an area that is small compared to the dimensions of the fluorescence, the atomic density is constant over the area corresponding to the detected region, and the fluorescence signal can be written as

$$S^{**} \propto \int_{-L}^{+L} n^{**}(x) e^{-\int_x^L \sigma n^*(x')dx'} dx , \tag{6}$$

where x is the direction perpendicular to the detection plane, σ is the cross section for photoabsorption, and transitions from Ba** atoms with density n^{**} terminate on atoms with density n^*. For fluorescence that is confined to a small region at the center of the cell, so that the lower limit in the x' integral in Eq. (6) can be replaced by 0, this relation is simplified considerably,

$$S^{**} \propto T \int_{-L}^{+L} n^{**}(x)dx , \tag{7}$$

where T is the transmission of the fluorescence from the center to the end of the cell. In this experiment, Eqs. (6) and (7) typically yield results that differ by $<1\%$. The ratios of the measured signals (in watts) from the Ba** and $6P$ atoms can be written as

$$\frac{S^{**}}{S_P} = \frac{\lambda_P \epsilon^{**} A^{**} T^{**} \int n^{**}(V)dV}{\lambda^{**} \epsilon_P A_P T_P \int n_P(V)dV} , \tag{8}$$

where the subscript P indicates the $6\,^3P_1$ level, and the superscript $**$ refers to the Ba** levels. ϵ is the efficiency per watt of the monochromator and photomultiplier tube (PMT) at a selected wavelength, and A is the atomic transition probability. Combining Eqs. (5) and (8), the energy-pooling rate coefficient will be determined from the data, without the knowledge of n^{**}, using

$$k = \frac{2S^{**}\lambda^{**}\epsilon_P A_P T_P \int n_P(V)dV}{B^{**} S_P \lambda_P \epsilon^{**} T^{**} n^{*2}(V)dV} , \tag{9}$$

where B^{**} is the fraction of Ba* radiatively branching into the detected transition.

III. APPARATUS

A description of the experimental apparatus is necessary for an understanding of the measurements that yield the EP rate coefficients. The experimental arrangement is shown in Fig. 2(a). The pump laser is a cw diode laser tuned to the 791-nm intercombination line of barium. After the laser beam is expanded, it is sent through a 3-mm-diameter aperture, and 3 mW is incident on the barium vapor. The laser diode is tuned using a grating-terminated cavity and its linewidth is less than 10 MHz. In order to excite a larger fraction of the atoms within the 700-MHz Doppler distribution to the $6P$ level, the laser injection current is modulated to sweep the laser frequency rapidly back and forth over the Doppler profile, with a sweep amplitude of 100 MHz and at a rate of 2 MHz. At buffer gas pressures (P_B) above ≈ 1000 Pa, this laser modulation has a negligible effect, since the pressure broadening then gives each atom an absorption

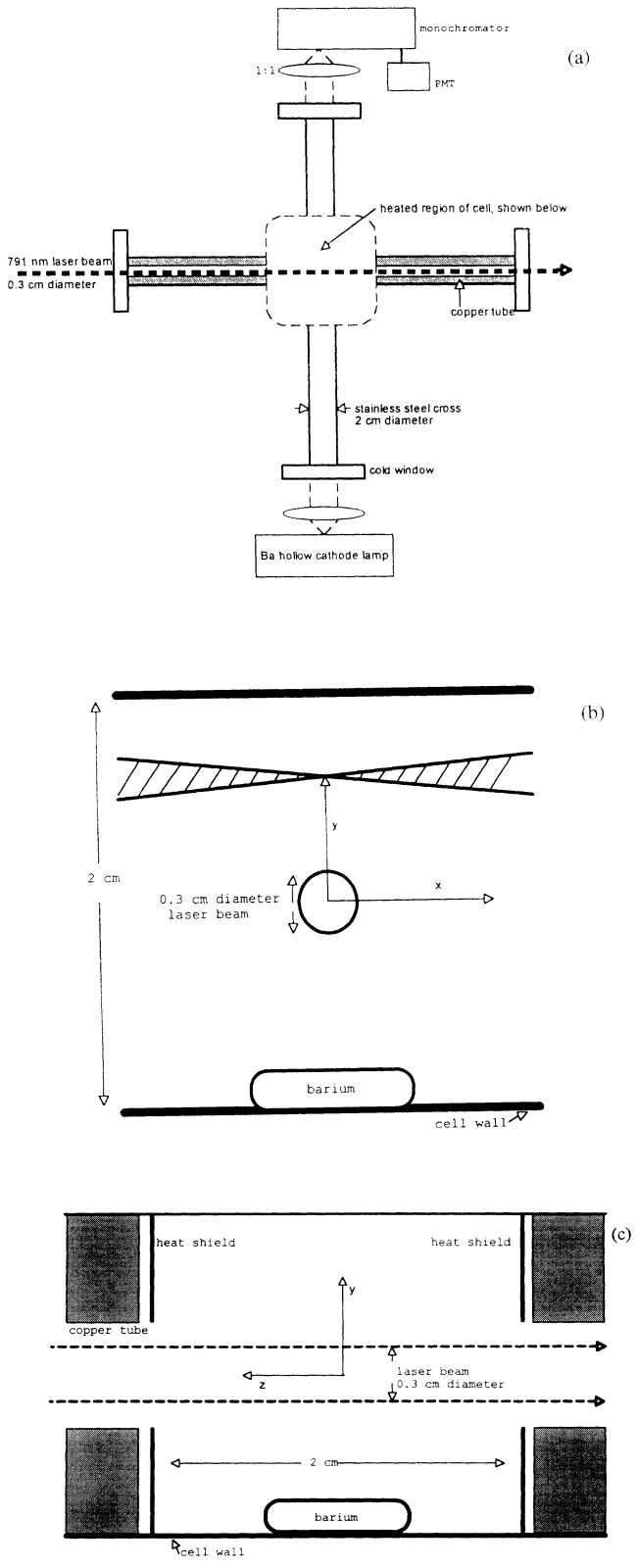

FIG. 2. Experimental arrangement. (a) gives a cross section of top view, where only the cross-shaped cell is drawn to scale. (b) shows the heated region of a cell, seen from the direction of the laser. The cross-hatched area is the region imaged by the monochromator when the entrance slit is imaged at the height y above the center of the cell. (c) illustrates the heated region of the cell, seen perpendicular to the laser.

width on the order of the width of the modulated laser [9].

Fluorescence emission and light from the barium hollow-cathode lamp are imaged with a PMT attached to a $\frac{3}{4}$ meter monochromator. The light from the hollow-cathode lamp is spread to fill the whole region that can be imaged by the monochromator. The vertical spatial distribution of the fluorescence intensity and the metastable density can be determined by imaging a narrow, horizontal monochromator slit (0.2-mm width, 0.2-cm length) into different regions of the cell [Fig. 2(b)].

A buffer gas confines the barium atoms in a heated, cross-shaped cell with cold windows on each of the four arms [Fig. 2(a)]. The cell is heated only in the center, and the buffer gas serves to prevent Ba atoms from reaching the cold windows. In the direction of the laser, copper tubes that make a thermal contact with the cold regions of the cell are inserted into the arms to reduce the amount of Ba vapor in these two cell arms, where fluorescence cannot be detected. Furthermore, stainless-steel heat shields are placed in the cell in order to define a 2-cm length of heated Ba vapor [Fig. 2(c)]. The heated region of the cell is illustrated from a perspective perpendicular to the laser [Fig. 2(b)] and in the direction of the laser [Fig. 2(c)].

Energy pooling was examined in several buffer gases and over pressures ranging from 13 to 13 000 Pa, as measured by a capacitance manometer. Although EP was examined in Kr, He, and Ne, the differences were small, and all measurements reported here were made with a Ne buffer gas. The experiment was carried out at 860 K, where the Ba density was $\sim 10^{12}/\text{cm}^3$ and the low-power laser absorption was 50%. Since there was a constant flux of barium atoms out to the cell walls, the barium vapor pressure was expected to be below the equilibrium value by a factor of 2–4. Our measurements were consistent with other studies [9,10] that found the barium vapor pressures reported in the Nesmayanov tables [11] to be approximately an order of magnitude too large. From 500 to 900 K, we measured Ba vapor pressures to be a factor of 2.5 lower than the equilibrium vapor pressure of Hinnov and Ohlendorf's [10].

IV. Ba* MEASUREMENTS

Rate equations for EP are determined from the measured values of n^* and from EP to intercombination line (S^{**}/S_P) fluorescence intensity ratios, using Eq. (8). To separate the contribution to energy pooling from different Ba* states (^1D, ^3D, and ^3P), these three densities and the $6s6p(^3P_1)$ fluorescence intensity were measured both as a function of position and as a function of buffer gas pressure. A study of n^* for the three Ba* levels is presented first, where Ba*(^3D) is the sum over J of Ba*(^3D_J).

Absorption of lines from the hollow-cathode lamp that terminate on the $6P$ and $5D$ levels were used to determine the Ba* density as a function of buffer-gas pressure and position. As shown in Fig. 2(b), hollow-cathode lamp light is perpendicular to the laser in the x direction and measures density as a function of the height y above or below the laser beam. In the present case of a low-power

lamp, the path integral of the density could be determined as

$$[\text{transmission fraction } (y)] = \frac{\int d\omega I_0(\omega) e^{-q(\omega)\int_{-L}^{L} n(x,y)dx}}{\int I_0(\omega) d\omega}, \quad (10)$$

where $q(\omega)$ is the frequency-dependent absorption cross section for the Ba* atoms. The hollow-cathode lamp emits light with 300-K Doppler line shapes [5], and at low P_B, the atoms have a 860-K Doppler distribution. Equation (10) was evaluated for the absorption of a 300-K Doppler line shape $I_0(w)$ by atoms with a 860-K Doppler line shape, as done by Mitchell and Zemansky [12].

While the Ba* density was nearly constant along the 2-cm laser path, its spatial distribution in the radial direction (perpendicular to the laser) was not constant. Absorption of lines from the barium hollow-cathode lamp was measured as a function of height (y) above the laser beam, as shown in Fig. 2(b). Since the laser beam excited a cylinder of atoms in the cell, and most EP (proportional to n^{*2}) occurs near the center of the cell, the distribution of n^* is close to cylindrically symmetric in the significant region. Thus, Eq. (10) was used to obtain $n^*(y) = \int n^*(x,y)dx$, and an Abel inversion [13] was used to find the radial distribution $n^*(r)$ from $n^*(y)$.

A. ^3P_J levels

The $6s6p(^3P_1)$ level is populated by laser excitation from the ground state, and it is depleted primarily through radiative decay to the ground state and to the $5D$ level. Typical $6P$ densities were 2×10^{10} cm^{-3}, the diameter of the region of excited atoms was approximately 0.3 cm, and absorption cross sections for lines terminating on the $6P$ level were approximately 5×10^{-12} cm^2. Thus, the lamp absorption for lines terminating on the $6s6p(^3P_1)$ level was only a few percent.

Hollow-cathode lamp lines were also used to search for absorption from the $6s6p(^3P_{0,2})$ levels resulting from intramultiplet collisional mixing, but the detection sensitivity precluded a careful study of intramultiplet mixing. Although the thermal equilibrium ratio of $6s6p(^3P_{0,1,2})$ is (0.39):1:(0.62), less than 1% absorption of lines from the hollow-cathode lamp was found from these levels. Using lifetimes derived from oscillator strengths calculated by Bauschlicher *et al.* [14] of 2.4 μs for $^3P_0$ and 1.3 μs for $^3P_2$, an upper limit of 10^{-11} cm^3 s^{-1} is estimated for the rate coefficient for neon collisional mixing from the $^3P_1$ to the $^3P_{0,2}$ levels. This lack of significant collisional mixing between the $6s6p(^3P_J)$ levels is consistent with the lack of evidence for intramultiplet mixing in the $\text{Ba}(^3P_J)$ levels found by Breckenridge and Merrow [15] and the small rate coefficient (typically 4 orders of magnitude below gas kinetic rates) found for intramultiplet mixing in the 5^3P_J levels in Sr [16].

Since the radiative decay rate for the 6^3P_1 level (0.82×10^6 s^{-1} [17]) was faster than the experimental diffusion rate, the $6P$ atoms are confined primarily to the laser volume, as seen in Fig. 3(a). As shown in Fig. 4, $n^*(6P)$ is nearly constant for $P_B < 100$ Pa, but it decreases for higher P_B. This decrease above 100 Pa is caused by the depletion of the ground state within the laser beam, due to metastable production. Once the ground state is depleted, the number of atoms that can be excited to the $6P$ levels is reduced, and the $6P$ density decreases. This is discussed in greater depth below, in the analysis of the $5D$ levels.

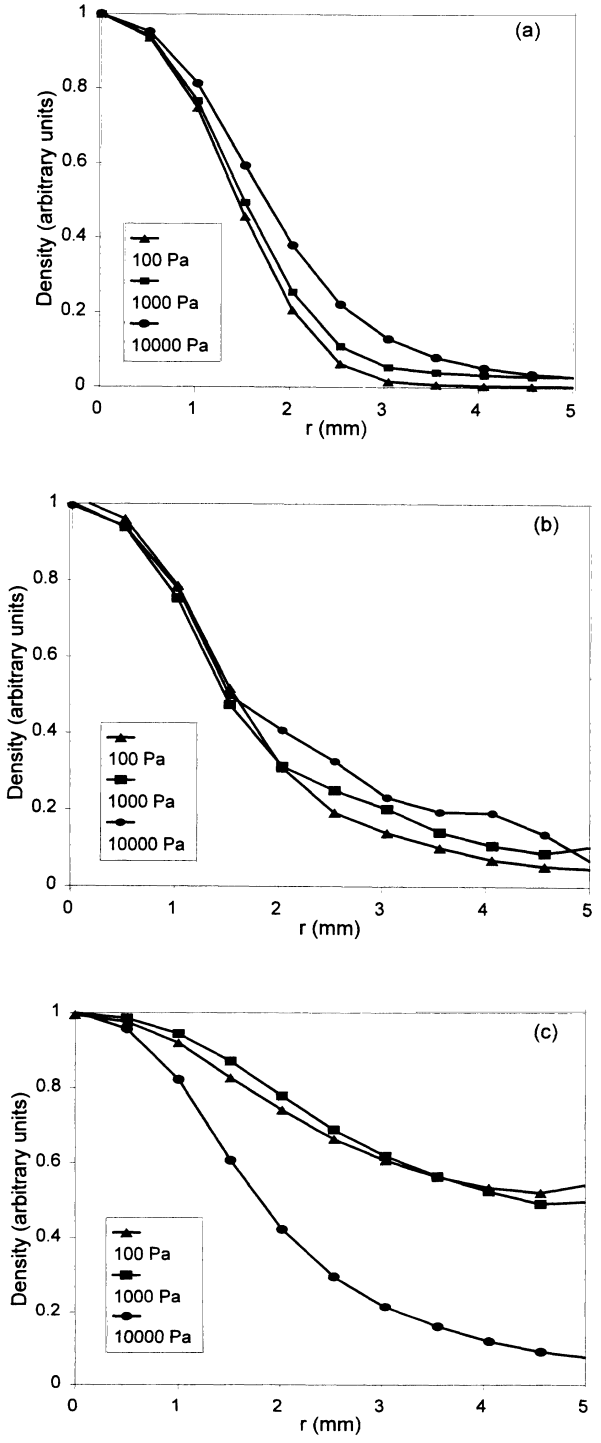

FIG. 3. Radial distribution of (a) 6^3P_1, (b) 5^1D_2, and (c) 5^3D_J excited barium atoms for three different values of P_B. Laser beam has 1.5-mm radius.

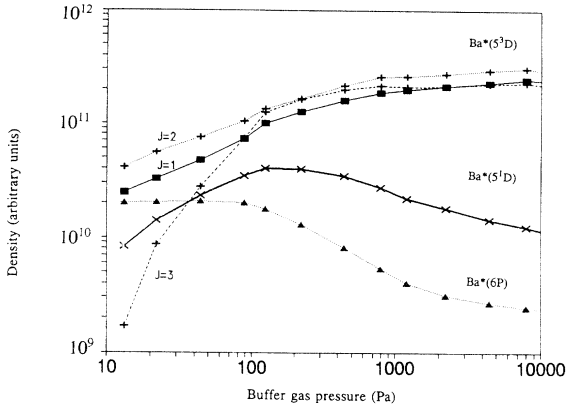

FIG. 4. Ba* densities as a function of P_B at $r=0$.

B. $5\,^1D_2$ level

The $5\,^1D_2$ level is produced primarily by collisional transfer from the $6P$ level. Evidence for this is found at lower buffer gas pressures, where $n^*(6P)$ is constant, and $n^*(5\,^1D)$ is proportional to buffer gas pressure. Because the $5\,^1D$ level is calculated to have a 0.25-s radiative lifetime [18], diffusion to the walls [19] and collisional quenching are its primary losses. Since the $5\,^1D$ level is found confined mostly to the laser volume [Fig. 3(b)], this indicates that collisional quenching of $5\,^1D$ is more rapid than that of $5\,^3D$. If this quenching were not present, $5\,^1D$ would be detected over the whole cell, similar to the $5\,^3D$ state at 1000 Pa in Fig. 3(c).

For 300 Pa $< P_B <$ 10 000 Pa, $n^*(5\,^1D)$ decreases (Fig. 4). This occurs because the $5\,^1D$ level is produced by collisional transfer from the $6P$ level, and the latter decreases above $P_B = 100$ Pa (Fig. 4).

Although all the mechanisms for the production and destruction of the $5\,^1D$ level have not been quantitatively characterized, the spatial distribution and buffer-gas dependence of $n^*(5\,^1D)$ are known and are unique. The $5\,^1D$ and $6P$ levels are confined mostly to the laser volume, whereas the $5\,^3D$ levels are spread throughout the cell.

C. $5\,^3D_J$ levels

The metastable $5\,^3D_{1,2}$ are produced primarily by fluorescence from the $6P$ level, and are lost primarily by diffusion to the walls. Radiative lifetimes of these levels are on the order of minutes [18]. As buffer-gas pressure increases, diffusional losses decrease, and consequently there is an increase in the $5\,^3D_J$ density. At $P_B > 100$ Pa, a majority of the atoms are loaded into the metastable levels, and less than 10% of the atoms are left in the ground state in the laser volume. These findings agree with the findings of Ehrlacher and Huennekens [9], who found over half of the atoms in the $5D$ levels, and Carlsten [20], who found the ground state 80% depleted. However, in the present experiment, we discovered that only half of the depleted atoms reside in the $6P$ and $5D$ levels. It is thought that atoms are also loaded into the $5d^2(^3F_J)$ and $5d^2(^1G_4)$ metastable levels [21] by EP, although no such populations were detected since we were unable to examine these levels in the current experiment.

The $5\,^3D$ metastables can also be quenched by collisions with ground state Ba atoms [22], and at higher buffer-gas pressures, this is seen to be the dominant loss mechanism for the $5\,^3D$ levels. This occurs mostly outside the laser excited region, where the ground state is not depleted. This explains the more confined spatial distribution of the $5\,^3D$ atoms at high buffer-gas pressure seen in Fig. 3(c): Metastables are not quenched as rapidly inside the laser volume, where the ground state (n) is depleted, as they are outside of this volume, where $n > n^*$.

The $5\,^3D$ levels display a unique buffer-gas dependence and spatial distribution. At lower buffer-gas pressures they diffuse over much of the cell, whereas they become more confined to the laser volume at higher buffer-gas pressures [Fig. 3(c)]. Furthermore, their density increases monotonically as buffer-gas pressure increases (Fig. 4). EP from $6P$ and $5\,^1D$ levels has a different spatial character than that from $5\,^3D$, and they can be separated on that basis. The EP from $6P$ versus that from $5\,^1D$ can be separated by their different n^* dependence on buffer-gas pressure. Using an infinite cylinder diffusion equation and including collisions, a computer model of the $6S$, $6P$, $5\,^1D$, and $5\,^3D$ densities revealed the same type of spatial and buffer-gas dependence that has been measured here.

V. EP FLUORESCENCE INTENSITY

Ba** fluorescence intensity was also measured as a function of position in the cell and buffer-gas pressure (Fig. 5). By comparing the buffer-gas dependence and spatial distributions of the EP fluorescence intensity with $(n^*)^2$ of various pairs of Ba* states, it is possible to isolate the EP contributions from each of three Ba* pairs. Although there are six possible Ba* pairs (when the $5\,^3D_J$ levels are summed and treated as one state), rate coefficients for only three Ba* pairs were determined. The rate coefficients for EP from $5\,^1D + 5\,^3D$ and $5\,^1D + 6P$ collisions could only be assigned upper limits, while rate coefficients for collisions between two Ba* atoms in the same state were clearly isolated.

The relative spectral sensitivity of the monochromator and PMT are calibrated as in previous experiments [5]. Since the metastable atom density can be large and diffuses throughout the cell, and most of the detected Ba** lines terminate on the metastable levels, the EP fluorescence can be significantly attenuated [$T^{**} < 1$ in Eq. (9)]. The distance from the center of the cell to the monochromator is half the full length of the cell, and Ba** populates a small region in the center of the cell. Since $T^{**} \propto e^{-\sigma n l}$, where σ is the absorption cross section and l is the length over which the light is absorbed, the transmission of the hollow-cathode lamp lines from the center of the cell to the monochromator is the square root of the transmission through the full length of the cell. The transmission of EP fluorescence can then be determined by correcting the 300-K lamp transmission for the 860-K Doppler line shapes of the atomic emitters and absorbers, as done by Mitchell and Zemansky [12].

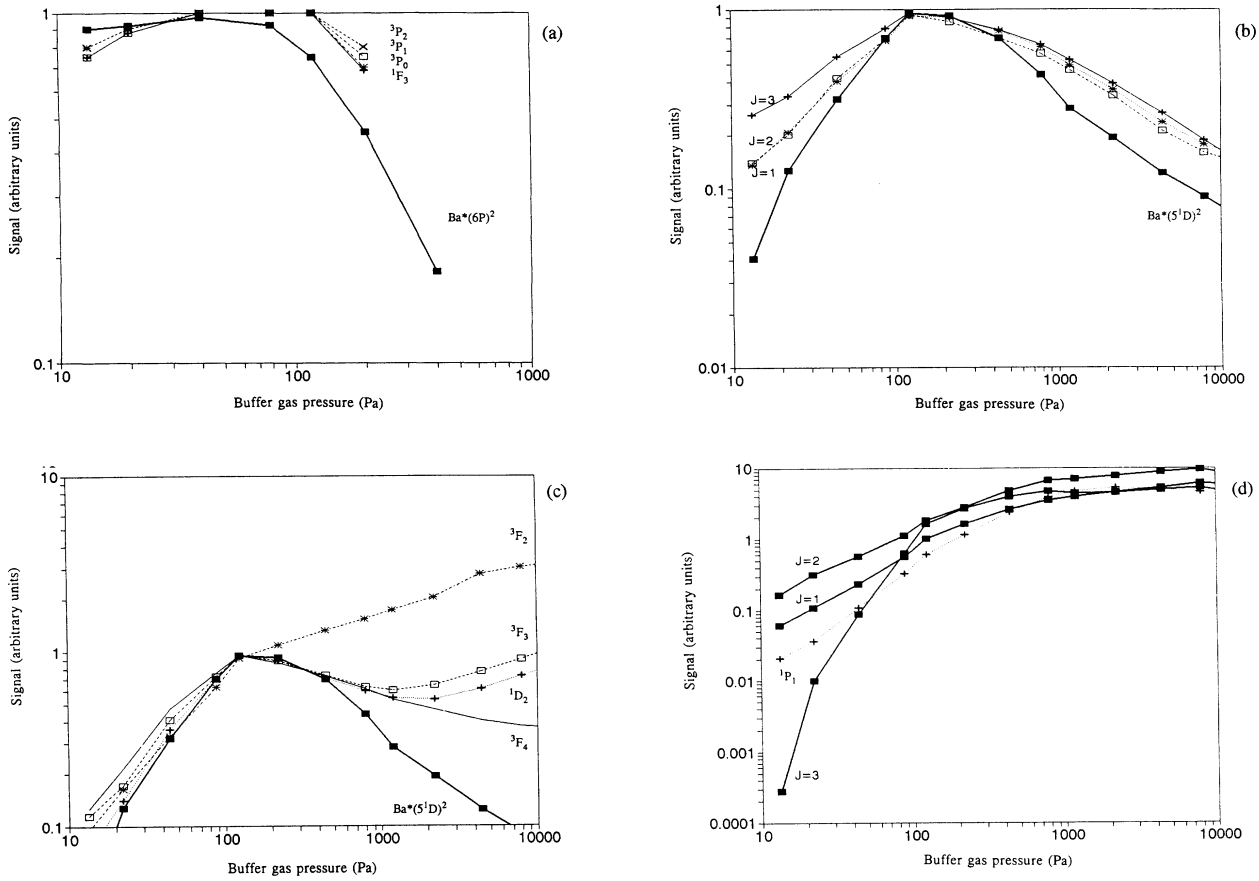

FIG. 5. P_B dependence of EP fluorescence signals compared to $(n^*)^2$; (a) $5d6p(^3P_J,^1F_3)$ compared to $Ba^*(6P)^2$; (b) $5d6p(^3D_J)$ compared to $Ba^*(5\,^1D)^2$; (c) $5d6p(^3F_J,^1D_2)$ compared to $Ba^*(5\,^1D)^2$; and (d) $6s6p(^1P_1)$ compared to $Ba^*(5\,^3D_J)^2$ for all three J levels.

T_P in Eq. (9) is determined for laser absorption. Generally, the experimental conditions produced $T^{**}>0.8$ and $T_P>0.55$, so uncertainties in these factors are relatively minor. Radiative branching ratios for the Ba** levels and the atomic transition probability for the intercombination line are required for a determination of absolute rate coefficients, and atomic transition probabilities for transitions which connect with the metastables must be used to determine the density of metastable atoms. These values have been obtained from published research [23–26].

We will first correlate the Ba** fluorescence from the $5d6p(^3P_{2,1,0})$ and $5d6p(^1F_3)$ levels to collisions of a pair of $6P$ atoms, as shown in Fig. 5(a). For $P_B<100$ Pa, both $(n^*)^2$ for the $6P$ state and the Ba** fluorescence intensity from these four levels are nearly constant, while $(n^*)^2$ for the metastables increases by more than a factor of 10 [Figs. 5(b) and 5(d)]. A more careful examination reveals that for P_B from 13 to 100 Pa, the fluorescence from the $5d6p(^3P_{2,1,0})$ and $5d6p(^1F_3)$ levels increases by 20%, while $n^*(5\,^1D)^2$ increases by 2500%. From this analysis alone, the $5\,^1D$ EP contribution to $5d6p(^3P_{2,1,0})$ fluorescence is shown to be $<1\%$. Similar arguments eliminate the possibility of significant contributions to these states at low P_B from $6P+5D$ or $5D+5D$ collisions. At $P_B>100$ Pa, the $n^*(6P)^2$ and the $5d6p(^3P_J,^1F_3)$ fluorescence decrease together, while $n^*(5D)^2$ are again different. Additionally, both the EP fluorescence intensity and $n^*(6P)$ are confined to the laser volume, while the 5^3D metastables are diffused over much of the cell. Consequently, the following reactions are detected:

$$Ba^*(6\,^3P_1)+Ba^*(6\,^3P_1)\rightarrow Ba^{**}(5d6p[^3P_J,^1F_3])+Ba(6\,^1S_0)+\Delta E\ . \quad (11)$$

Rate coefficients for these reactions are listed in Table I. The volume integrals in Eq. (9) that are used to obtain these rate coefficients use the spatial distribution of n^* data shown in Fig. 3(a). It is interesting to note that no fluorescence intensity was observed from the $6s6p(^3S_1)$ level, such that an upper limit of 10^{-11} cm^3 s^{-1} can be put on the rate coefficient for EP to these states. The radiative branching of the $6s6p(^3S_1)$ level and the decreased sensitivity of our PMT for these infrared transitions (7195–7906 Å) hampered our ability to better determine this upper limit.

Next, we will consider the EP fluorescence from the $5d6p(^3D_J,^1D_2,^3F_{3,4})$ levels. Using arguments similar to those presented above, these levels are shown to be produced by collisions between $5\,^1D$ atoms. As seen in Figs. 5(b) and 5(c), fluorescence from these three sets of levels

TABLE I. Energy-pooling rate coefficients k (10^{-11} cm^{3}s^{-1}) at 860 K to the Ba** level from collisions between pairs of $6P$ atoms, where twice the $6P$ energy is 25 273 cm^{-1}.

Ba** level	Energy defect (cm^{-1})	Wavelength (Å)	Branching ratio	$k(e^{\Delta E/kt})/g^{**}$	k (cm^{3}s^{-1})
$5d6p\ ^1F_3$	+1540	6483	0.85	1.9	1.0
$5d6p\ ^3P_2$	+680	6111	0.72	1.2	2.0
$5d6p\ ^3P_1$	+430	6063	0.63	1.5	2.2
$5d6p\ ^3P_0$	+370	6019	1	1.3	0.70

TABLE II. Energy-pooling rate coefficients k (10^{-11} cm^{3}s^{-1}) at 860 K to the Ba** level from collisions between pairs of $5\ ^1D$ atoms, where twice the $5\ ^1D$ energy is 22 791 cm^{-1}.

Ba** level	Energy defect (cm^{-1})	Wavelength (Å)	Branching ratio	$k(e^{\Delta E/kt})/g^{**}$	k (cm^{3}s^{-1})
$5d6p\ ^3D_3$	+2190	6499	0.50	55	10
$5d6p\ ^3D_2$	+1740	6527	0.54	31	8.5
$5d6p\ ^3D_1$	+1400	6595	0.64	28	8.0
$5d6p\ ^3F_4$	+970	7060	1	7.8	14
$5d6p\ ^3F_3$	+160	7280	0.81	3.7	20
$5d6p\ ^1D_2$	+280	7120	0.34	3.8	12

TABLE III. Energy-pooling rate coefficients k (10^{-11} cm^{3}s^{-1}) at 860 K to the Ba** level from unseparated $6P+6P$ or $6P+5\ ^1D$ collisions. The rate coefficients represent an upper limit from the assumed Ba* collision pair.

Ba** level	Assumed Ba* pair	Energy defect (cm^{-1})	Wavelength (Å)	Branching ratio	k (cm^{3}s^{-1}) Upper limit
$5d6p\ ^3D_3$	$6P+6P$	−290	6499	0.50	19
$5d6p\ ^3D_3$	$5\ ^1D+6P$	+950			20
$5d6p\ ^3D_2$	$6P+6P$	−740	6527	0.54	8.0
$5d6p\ ^3D_2$	$5\ ^1D+6P$	+500			8.6
$5d6p\ ^3D_1$	$6P+6P$	−1080	6595	0.64	7.5
$5d6p\ ^3D_1$	$5\ ^1D+6P$	+160			8.1

TABLE IV. Energy-pooling rate coefficients k (10^{-11} cm^{3}s^{-1}) at 860 K to the Ba** level from unseparated $5\ ^3D+5\ ^3D$, $5\ ^1D+5\ ^1D$, or $5\ ^1D+5\ ^3D$ collisions. The rate coefficients represent an upper limit from the assumed Ba* collision pair.

Ba** level	Assumed Ba* pair	Energy defect (cm^{-1})	Wavelength (Å)	Branching ratio	k (cm^{3}s^{-1}) Upper limit
$5d6p\ ^3D_3$	$5\ ^3D+5\ ^3D$	+6270	6499	0.50	0.014
$5d6p\ ^3D_3$	$5\ ^1D+5\ ^3D$	+4230			0.37
$5d6p\ ^3D_2$	$5\ ^3D+5\ ^3D$	+5820	6527	0.54	0.018
$5d6p\ ^3D_2$	$5\ ^1D+5\ ^3D$	+3780			0.48
$5d6p\ ^3D_1$	$5\ ^3D+5\ ^3D$	+5480	6595	0.64	0.021
$5d6p\ ^3D_1$	$5\ ^1D+5\ ^3D$	+3440			0.54
$5d6p\ ^3F_4$	$5\ ^3D+5\ ^3D$	+5050	7060	1	0.040
$5d6p\ ^3F_4$	$5\ ^1D+5\ ^3D$	+3010			1.0
$5d6p\ ^3F_3$	$5\ ^3D+5\ ^3D$	+4240	7280	0.81	0.080
$5d6p\ ^3F_3$	$5\ ^1D+5\ ^3D$	+2200			2.1
$5d6p\ ^3F_2$	$5\ ^3D+5\ ^3D$	+3350	7672	0.50	0.67
$5d6p\ ^3F_2$	$5\ ^1D+5\ ^3D$	+1310			1.7
$5d6p\ ^3F_2$	$5\ ^1D+5\ ^1D$	−730			34
$5d6p\ ^1D_2$	$5\ ^3D+5\ ^3D$	+4360	7120	0.34	0.043
$5d6p\ ^1D_2$	$5\ ^1D+5\ ^3D$	+2320			1.1

TABLE V. Energy-pooling coefficients k (10^{-11} cm^3 s^{-1}) at 860 K to the Ba** level from collisions between pairs of $5\,^3D$ atoms, where twice the $5\,^3D$ energy is 18714 cm^{-1}.

Ba** level	Energy defect (cm^{-1})	Wavelength (Å)	Branching ratio	k (cm^3 s^{-1})
$6s6p_1P_1$	+654	5536	0.9966	>0.81

nearly matches the P_B dependence of $n^*(5\,^1D)^2$, and no other Ba* pair in the 100 Pa $< P_B <$ 1000 Pa region where $n^*(5\,^1D)$ is largest. Furthermore, these emissions are confined to the laser volume, as is $n^*(5\,^1D)$. Using this 100 Pa $< P_B <$ 1000 Pa data, we have determined the rate coefficients for these reactions shown in Table II. At $P_B <$ 100 Pa, $n^*(5\,^1D)^2$ decreases faster than the Ba** intensities in Fig. 5(b). Since $n^*(6P)$ is largest at low P_B, this suggests additional contributions to EP from either $6P+6P$ or $6P+5\,^1D$ collisions. However, these two possibilities could not be separated due to an insufficient P_B range, and because the $6P$ and $5\,^1D$ atoms have indistinguishable spatial characteristics (they are confined to the laser volume). We can give upper limits for EP rate coefficients to these states from $6P+5\,^1D$ collisions or from $6P+6P$ collisions (Table III), recognizing that one or the other is probably equal to this upper limit. At $P_B >$ 1000 Pa, $n^*(5\,^1D)^2$ again decreases faster than the Ba** intensities, suggesting additional contributions to EP from either $5\,^3D+5\,^3D$ or $5\,^3D+5\,^1D$ collisons, since the $5\,^3D$ metastables predominate at higher P_B. Again, they cannot be clearly separated, and upper limits for EP rate coefficients from $5\,^3D+5\,^3D$ or $5\,^1D+5\,^3D$ collisions are given in Table IV.

Just as the square of the $5\,^3D$ metastable density increases as P_B increases, so does the fluorescence intensity from the $6s6p(^1P_1)$ level [Fig. 5(d)]. Additionally, the spatial distribution of the $6s6p(^1P_1)$ fluorescence matched $n^*(5\,^3D)^2$: They were both spread over the whole cell at lower P_B, and they became more confined to the center at higher P_B. Thus, the production of $6s6p(^1P_1)$ from a pair of ^3D levels was clearly observed. However, the resonance line is severely trapped (optical depth of about 200), and the geometry of the cross-shaped cell is not simple, so the fluorescence is expected to escape in a highly anisotropic manner. In addition, three different ^3D_J sublevels were present, and each level's contribution to EP could not be isolated. Thus, a rate coefficient for the energy pooling to $6s6p(^1P_1)$ from a pair of ^3D levels could not be determined. As a consequence of the longer Ba-filled distance between cell center and spectrometer, we expect less than an isotropic average of Ba*$(6\,^1P_1)$ emission to be detected. Thus, if one assumes the light escapes isotropically and uses the sum of the ^3D_J densities in $(n^*)^2$, a minimum for the energy-pooling rate coefficient can be determined (Table V). Similarly, fluorescence intensity was observed from the $5d6p(^3F_2)$ level, but its buffer-gas dependence indicated that it resulted from a combination of $5\,^1D+5\,^1D$, $5\,^1D+5\,^3D$, and $5\,^3D+5\,^3D$ collisions, and the contribution from each pair could not be isolated. Upper limits for EP rate coefficients to the $5d6p(^3F_2)$ level from $5\,^1D+5\,^3D$, $5\,^3D+5\,^3D$ or $5\,^1D+5\,^1D$ collisions are given in Table IV. In each case, either one or a combination of rate coefficients must be near this limit.

Several other energy levels were likely to have been populated by energy-pooling collisions, but their infrared fluorescence wavelengths were inaccessible with this detection system. In particular, the $5d^2(^3P_J,\,^1D_2,\,^3F_J,\,^1G_4)$ states have energy defects of only a few hundred cm^{-1} from a pair of $^1D_2$ levels.

VI. CONCLUSION

Uncertainties in the Ba* density are significant, since the rate coefficient for EP is proportional to (Ba*)^2. Uncertainties can arise from an improper determination of the path length of absorption and from hollow-cathode line shapes that differ from the assumed 300-K Doppler distribution. Resulting uncertainties in Ba* densities are estimated to be ~10%. The intercombination line atomic transition probability is given by Parkinson and Tomkins [26] to 22%, and the branching ratios are known to about 10% [23–25]. Other small experimental errors arise from measuring the ratios of the fluorescence intensities. While contributions to rate coefficients from different Ba* atoms has been largely isolated, the resolution may not be complete, and some small background contribution from other unresolved colliding pairs of Ba* atoms may lead to inaccuracies in the determination of the rate coefficients. Overall, the uncertainties in the rate coefficients for energy pooling are estimated to be 50%.

Most of the EP rate coefficients measured here are within a factor of 10 of gas-kinetic collision rates. Other reported EP rate coefficients for Sr [3,4] and Na [1,2] have similar magnitudes. Energy-pooling rate coefficients are examined below as functions of total angular momentum L, total spin S, energy defect ΔE, and electron configuration.

In contrast to normal electronic energy transfer, the measured EP rate coefficients are remarkably independent of the energy defect. In this experiment, rate coefficients have been measured only for endothermic processes. Rate coefficients do not vary systematically for energy defects ranging from +156 cm^{-1} to +2200 cm^{-1} for pooling from a pair of $5\,^1D$ atoms (Table II). Similarly, there is little difference in the rate coefficients for pooling to the several $5d6p(^3P_J,\,^1F_4)$ levels from a pair of $6P$ atoms (Table I), despite energy defects ranging from 370 cm^{-1} to 1540 cm^{-1}. Yet, for energy defects over +1500 cm^{-1} and a thermal energy of ~600 cm^{-1}, only a small fraction of the atoms have enough kinetic energy to support these reactions. However, these energy-defect dependencies are somewhat biased because

the states with the greatest energy defects had the largest statistical weights. In spite of these relatively small rate coefficient differences from one Ba* pair, the rate coefficient from a $5\,^1D$ pair are typically 10 times larger than from a $6P$ pair.

There was no discernible spin dependency to the energy pooling, since pairs of $6\,^3P_1$ atoms and pairs of $5\,^1D_2$ atoms produced both triplet and singlet states in comparable amounts. If total spin were conserved, it would be impossible for a pair of singlet states to produce a triplet state. These spin-changing collisions, which have been previously observed for other alkaline earth pairs [5,6], are connected with the breakdown of LS coupling, which is severe for Ba. S and L are not good isolated-atom quantum numbers, and spin selection rules are not applicable in collisions.

Since a pair of $6P$ atoms produced a ^1F state but not a ^1S state, and a pair of $5D$ atoms were found to strongly produce F and D states but not P states, there is an indication that EP increases with L. However, this trend is tenuous in this experiment, since differing energy defects and statistical weights may have accounted for the apparent trend in L. Overall, no clearcut trends are discernable and no simple explanations of these results are apparent.

ACKNOWLEDGMENT

This work was supported by National Science Foundation Grant No. PHY90-12244 to the University of Colorado.

[1] M. Allegrini, P. Bicchi, and L. Moi, Phys. Rev. A **28**, 1338 (1983).
[2] S. A. Davidson, J. F. Kelly, and A. Gallagher, Phys. Rev. A **33**, 3756 (1986).
[3] L. Barbier and M. Cheret, J. Phys. B **16**, 3213 (1986).
[4] J. F. Kelly, M. Harris, and A. Gallagher, Phys. Rev. A **38**, 1225 (1988).
[5] H. C. G. Werij, M. Harris, J. Cooper, and A. Gallagher, Phys. Rev. A **43**, 2237 (1991).
[6] W. H. Breckenridge, W. L. Nikolai, and J. Stewart, J. Chem. Phys. **74**, 2073 (1981).
[7] S. Majetich, C. A. Tomczyk, and J. R. Wiesenfeld, Phys. Rev. A **41**, 6085 (1990).
[8] C. Gabbanini, S. Gozzini, G. Squadrito, M. Allegrini, and L. Moi, Phys. Rev. A **39**, 6148 (1989).
[9] E. Ehrlacher and J. Huennekens, Phys. Rev. A **47**, 3097 (1993).
[10] E. Hinnov and W. Ohlendorf, J. Chem. Phys. **50**, 3005 (1969).
[11] A. N. Nesmayanov, *Vapor Pressure of the Elements* (Academic, New York, 1963)
[12] A. C. G. Mitchell and M. W. Zemansky, *Resonance Radiation and Excited Atoms* (Cambridge Univeristy Press, Cambridge, 1934).
[13] W. L. Barr, J. Opt. Soc. Am. **52**, 885 (1962).
[14] C. W. Bauschlicher, R. L. Jaffe, S. R. Langhoff, F. G. Mascarello, and H. Partridge, J. Phys. B **18**, 2147 (1985).
[15] W. H. Breckenridge and C. N. Merrow, J. Chem. Phys. **88**, 2329 (1988).
[16] J. F. Kelly, M. Harris, A. Gallagher, Phys. Rev. A **37**, 2354 (1988).
[17] B. M. Miles and W. L. Wiese, At. Data **1**, 1 (1969).
[18] J. Migdalek and W. E. Baylis, Phys. Rev. A **42**, 6897 (1990).
[19] T. G. Walker, K. D. Bonin, and W. Happer, J. Chem. Phys. **87**, 660 (1987).
[20] J. L. Carlsten, J. Phys. B **7**, 1620 (1974).
[21] H. P. Palenius, Phys. Lett. **56A**, 451 (1976).
[22] P. G. Whitkop and J. R. Wiesenfeld, J. Chem. Phys. **72**, 1297 (1980).
[23] S. Niggli and M. C. E. Huber, Phys. Rev. A **39**, 3924 (1989).
[24] S. Niggli and M. C. E. Huber, Phys. Rev. A **35**, 2908 (1987).
[25] L. Jahreiss and M. C. E. Huber, Phys. Rev. A **31**, 692 (1985).
[26] W. H. Parkinson and F. S. Tomkins, J. Opt. Soc. Am. **68**, 534 (1978).

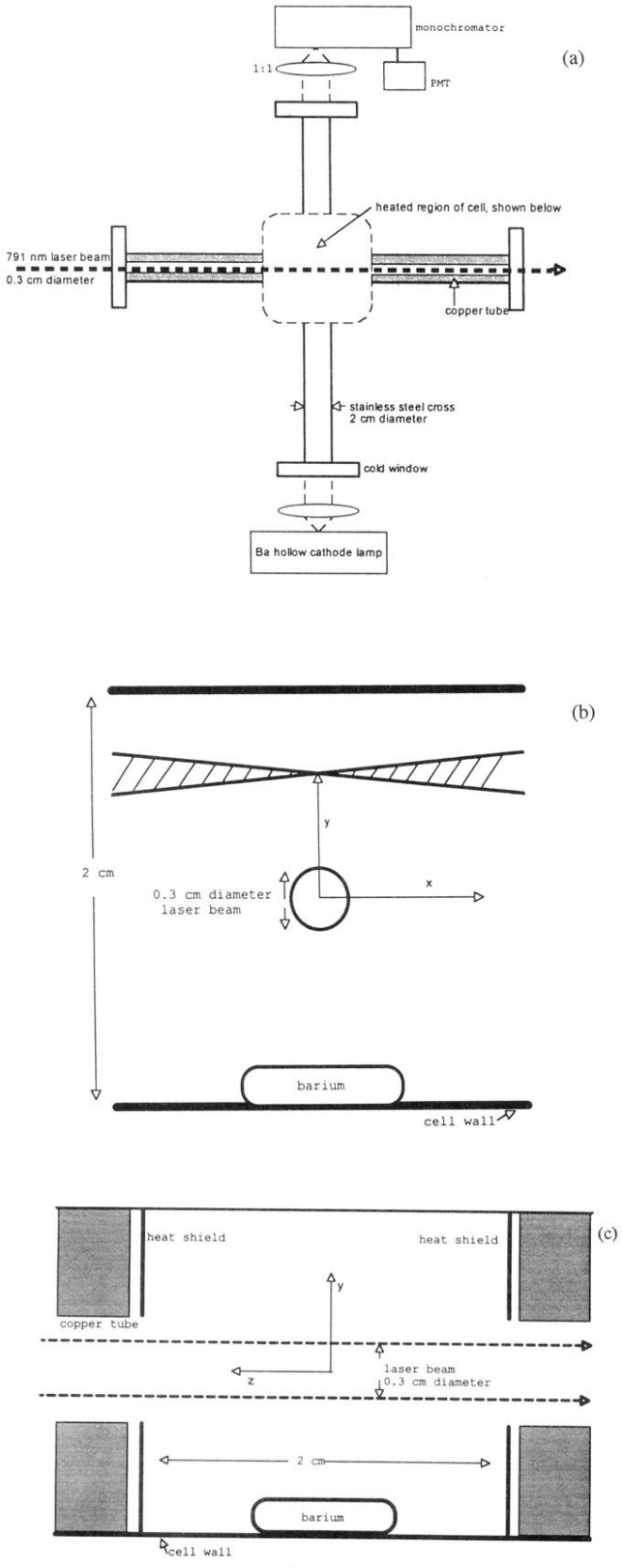

FIG. 2. Experimental arrangement. (a) gives a cross section of top view, where only the cross-shaped cell is drawn to scale. (b) shows the heated region of a cell, seen from the direction of the laser. The cross-hatched area is the region imaged by the monochromator when the entrance slit is imaged at the height y above the center of the cell. (c) illustrates the heated region of the cell, seen perpendicular to the laser.